Stable Dissipative Solitons in Semiconductor Optical Amplifiers

Erdem A. Ultanir and George I. Stegeman
CREOL/School of Optics, University of Central Florida, Orlando, Florida 32816, USA

Dirk Michaelis,* Christoph H. Lange, and Falk Lederer
Friedrich-Schiller-Universität Jena, Max-Wien-Platz 1, 07743 Jena, Germany
(Received 21 January 2003; published 27 June 2003)

We have observed for the first time stable spatial solitons in semiconductor optical amplifiers. Soliton destabilization due to the growth of background noise was suppressed by using patterned electrodes on the device. Numerical simulations fit very well with the experiment results. We show that it is possible to excite these solitons with about 60 mW input power.

DOI: 10.1103/PhysRevLett.90.253903 PACS numbers: 42.65.Tg, 05.45.Yv, 47.20.Ky

Spatiotemporal localization of dynamical excitations is a characteristic feature of a wide class of nonlinear systems. Beyond pattern formation in systems driven far from equilibrium [1] the formation and dynamics of isolated structures known as solitons or solitary waves have been in the focus of physical research during the past several decades. In nonlinear optics the study of light propagation in a variety of geometries, as, e.g., bulk materials, film waveguides, fibers, arrays of waveguides, and cavities has led to the observation of temporal, spatial, spatiotemporal, and discrete solitons (see [2–4], and references therein).

Here we are concerned with spatial solitons, which are formed by the mutual balance of diffraction and nonlinear phase modulation and can be divided into two subclasses, viz., propagating solitons, usually termed spatial solitons, and cavity solitons. Cavity solitons are localized transverse peaks in transmission or reflection. They strongly rely on the nonlinear interaction of forward and backward propagating fields where cavity (radiation) losses are compensated by gain or an external holding beam. Thus the underlying physical model does usually not conserve energy or any other quantity. Hence, cavity solitons belong to the class of dissipative solitons and have been observed in Fabry-Perot cavities or single mirror feedback setups [2,4]. They form a zero parameter family because their features, for example, amplitude, width, spatial profile, are completely determined by the system parameters.

In contrast to this, propagating spatial solitons (henceforth for the sake of simplicity we will call them spatial solitons) do not require any feedback mechanism and consist of forward propagating fields only. Up to now all experimentally verified spatial solitons of this type exist in Hamiltonian systems, where at least energy is conserved, and can thus be regarded as conservative solitons [2]. They form at least one parameter families, i.e., for a definite physical system, one of their parameters, either the soliton amplitude or spatial width, can be varied independently.

In this Letter we experimentally demonstrate for the first time the existence of stable dissipative (propagating) spatial solitons. In our experiments, which were carried out in a patterned semiconductor optical amplifier (SOA), we prove that, fixing the system parameters, this dissipative soliton is a stable attractor against changes of the input beam.

Besides this fundamental point of view, reconfigurable networks and all-optical switching could be achieved by making use of the fundamental concept of light guiding light based on the propagation of spatial solitons [5]. But the application of this concept in future all-optical information processing critically depends on meeting some essential requirements such as fast (a few ps) and low power (mW region) operation, simple and compact device geometry, simple interconnects to fiber systems, and the usage of standard technologies. Most of the previous experiments with spatial solitons [5], either in photorefractive media, which are very slow, or in quadratic or cubic nonlinear media, which require kW powers, have verified the basic principles but are very far from application. With respect to potential applications the most promising results were obtained for semiconductor cavity solitons [6,7]. Here we also take advantage of the huge carrier-induced nonlinearities of semiconductors but show propagating spatial dissipative soliton formation, which is more robust and simpler to achieve than in cavities. This is because no holding beam is needed and therefore less thermal effects appear. Moreover, these solitons are less sensitive with respect to spatial inhomogeneities and drift of system parameters, for example, sample length. Thus it is anticipated that semiconductor spatial solitons will have the potential for implementing beam steering, routing, and optical processing in optical communications at practical power levels (mW) with fast response times (ps). Suppression of filament formation, which is a serious problem in broad area semiconductor devices as a result of carrier-induced refractive index changes [8–10], is another potential field of application for this new kind of dissipative solitons. Although there

were some preliminary self-trapping experiments in SOAs [11], which have subsequently been proven to be unstable systems for soliton generation [12], to the best of our knowledge spatial solitons in semiconductor amplifiers have not been previously reported.

The stability of solitons is determined by the details of the operating conditions [13–15]. Their regions of stability can be evaluated from bifurcation diagrams that describe the solutions of the system-defining equations, obtained by changing the relevant control parameter, e.g., the system net gain. A subcritical bifurcation is one of the most common scenarios for finding stable dissipative soliton solutions (see Fig. 1), since the background field (low power soliton tails) experiences loss thus suppressing its destabilization.

In our case, the key to obtaining stable solitons is to provide loss regions, which act as saturable absorbers (SA), and gain regions, for which the saturation intensity is different. Thus the system gives a net gain or loss depending on the input intensity, and solitons are solutions where gain and loss are balanced. Previously we have shown theoretically that stable dissipative solitons should exist in bulk semiconductor optical amplifiers using a patterned electrode device [12]. These amplifiers have periodic electrodes (for electrical pumping) aligned perpendicular to the propagation direction (see inset of Fig. 1). A SOA/SA device can be modeled using two coupled equations [16,17] for the carrier density (N), and the TE polarized electric field (ψ). We normalize the carrier density by N_{tr}, the transparency carrier density, and the field by the saturation field level $|\psi_s|^2 = \hbar\omega d N_{\mathrm{tr}}/g$, where d is the quantum well (QW) width and g the effective gain coefficient. The normalized equations for the carrier density (N) and the field (ψ) take the form

$$\psi_z = \frac{i}{2}\psi_{xx} + \psi[f(N)(1 - ih) - \alpha], \tag{1}$$

$$DN_{xx} + \pi(z) - BN^2 - CN^3 - f(N)|\psi|^2 = 0, \tag{2}$$

where $f(N)$ is a function that describes the carrier dependent gain. It is assumed to be a linear function of N for bulk semiconductors, and logarithmic for the QWs. Here we assume $f(N) = \ln[(NN_{\mathrm{tr}} + N_s)/(N_{\mathrm{tr}} + N_s)]$. N_s is a fitting constant, h the linewidth enhancement (Henry factor), α is the internal loss which includes scattering losses and the cladding layer absorption, $\pi(z)$ the periodic pumping coefficient, D the carrier diffusion coefficient, B the spontaneous recombination coefficient, and C the Auger recombination rate. Normalized axes are used; z and x are defined as, $z = z_{\mathrm{real}}g$; $x = x_{\mathrm{real}}\sqrt{2\pi n g/\lambda_0}$

The SOA/SA device can be also described by a space-averaged model which couples the carrier densities in the pumped [N_1, $\pi(z) = \pi_0$] and unpumped regions [N_2, $\pi(z) = 0$] to the field equation. In first order approximation, the gain function $f(N)$ can be replaced by its averaged value $\overline{f}(N_1, N_2) = [f(N_1)w_1 + f(N_2)w_2]/(w_1 + w_2)$, where w_1 and w_2 are the widths of the pumped and unpumped regions. Nevertheless, we solved the full set of the three coupled differential equations [Eq. (1) for ψ and Eq. (2) for N_1 and N_2] for equal widths of pumped and unpumped regions ($w_1 = w_2$), by using parameters appropriate for an InGaAs semiconductor quantum well ($h = 3$, $\alpha = 0.024$, $N_{\mathrm{tr}} = 2.5 \times 10^{18}\ \mathrm{cm}^{-3}$, $N_s = 0.6 \times 10^{18}\ \mathrm{cm}^{-3}$, $d = 60$ Å $g = 104\ \mathrm{cm}^{-1}$, $\eta = 0.85$, $D = 3.311$, $B = 3.0$, and $C = 0.219$) [17,18]. Here we determined the stationary soliton solution $\psi(x)\exp(i\lambda z)$, which is independent of any initial condition, $\psi(x)$ is the soliton shape and λ is its propagation constant. Peak field values for the soliton solutions are plotted in Fig. 1 as a function of the small signal gain coefficient (δG) that is defined as the averaged net gain for the background ($\delta G = [\overline{f}(N_1, N_2) - \alpha]$ where N_1 and N_2 are calculated for $\psi \cong 0$ as the pumping level π is increased). The soliton solutions bifurcate subcritically ($\partial\psi/\partial\delta G < 0$) from the critical point $\delta G = 0$. Equation (1) also has trivial solutions $\psi = 0$, which are stable for $\delta G < 0$, and unstable for $\delta G > 0$. Stable solitons can appear only for $\delta G < 0$, since the background noise level has stable solutions ($\psi = 0$) in that region. We have estimated the threshold pumping current level for stable solitons to be $4A$ for a 300 μm wide and 1 cm long device.

These spatial solitons were investigated experimentally in a device fabricated on a p-n junction diode wafer

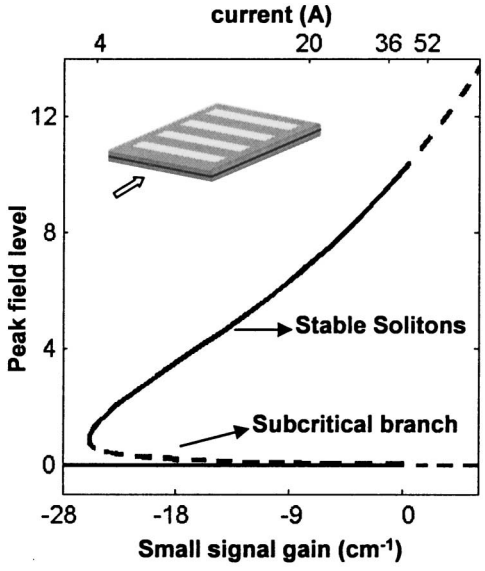

FIG. 1. Plot of peak field level ($\sqrt{\mathrm{mW}/\mu\mathrm{m}}$) of soliton solutions versus small signal gain δG. The dashed line shows the unstable solutions, and the dark line shows the stable solitons. Current values (x axis-top scale) are calculated assuming 300 μm width contact patterns on a 1 cm long device. (Current $I = \pi q d N_{\mathrm{tr}} A_{\mathrm{contact}}/\eta$, where $A_{\mathrm{contact}} = 300\ \mu\mathrm{m} \times 1\ \mathrm{cm} \times 0.5$). The inset shows a sample device with propagation direction along the arrow.

grown by molecular beam epitaxy. The wafer structure consists of a n-GaAs substrate with a n-GaAs buffer layer, a 100 nm graded n-$Al_xGa_{1-x}As$ ($x = 0.2$–0.36) layer, a 1 μm n-$Al_{0.36}Ga_{0.64}As$, and an 80 Å $In_{0.17}Ga_{0.83}As$ layer sandwiched between two symmetric waveguiding layers of 500 nm $Al_{0.2}Ga_{0.8}As$. Deposited on top are 1 μm p-$Al_{0.36}Ga_{0.64}As$, 100 nm graded p-$Al_xGa_{1-x}As$ ($x = 0.36$–0.2) and 400 nm p-GaAs contact layers. The peak electro-luminescence was found to occur at 946 nm at room temperature. Periodic Au contact stripes, 11 μm wide, and 300 μm long were separated by 9 μm SiN insulator stripes which form the unpumped absorption regions. The device length is about 1 cm. In order to avoid thermal effects, we used a pulsed current source (400 ns pulses at 1 kHz repetition rate). Stable temperatures ($\sim 21\,^{\circ}C$) for the device in repeated experiments are guaranteed by mounting them on a TE cooled copper mount.

Light input from a CW Ti:sapphire laser is shaped with a 2 lens elliptical telescope. We used a 40× microscope objective to couple the laser beam into the waveguide. Both focal regions [orthogonal and parallel to the waveguide] are carefully aligned to overlap after the microscope objective. This gives maximum coupling of light into the waveguide and a planar phase front at the input. The device is tilted about 2° from normal incidence to avoid any back reflections. The output of the sample is imaged onto a charge-coupled device camera with a microscope objective.

When a 16.5 μm FWHM beam is coupled into the waveguide at a wavelength of 965 nm where the material is transparent, we observed diffraction to 62 μm FWHM as a result of 3.6 diffraction lengths of linear propagation. As the wavelength is tuned inside the band gap ($\lambda <$ 955 nm), and current is injected into the device, a localized spatial output beam with a FWHM of 21 μm at 950 nm with 4A of current is seen [see Fig. 2]. Figure 3(a) shows the formation of such a localized beam. The device absorbs all the light until the current reaches 3.8A. After this point the system follows the stable subcritical bifurcation branch (see Fig. 1), and the peak intensity of the localized beam increases. The output profile does not show any formation of noise filaments up to 4.6A. At higher currents the amplified spontaneous emission increases above the subcritical branch, and generates noisy peaks on the sides of the soliton. By using a finite difference beam propagation method (FDBPM) [19] based on Eqs. (1) and (2), we calculated the progressive evolution of the light beam with distance for the patterned amplifier device. The simulations also support the bifurcating behavior of the solitons with the corresponding threshold pumping current, Fig. 3(b), which indicate the turning point in the bifurcation diagram.

Next we will confirm that the spatial soliton is a dissipative one. Therefore for fixed values of system parameters the soliton is a stable attractor and no families of solitons exist. In the region of attraction an arbitrary initial input beam will always converge towards one, distinct soliton. By using a half wave plate and a polarizer we increased the input power and took pictures of the output, Fig. 4(a). Beyond 60 mW input power, the beam forms a localized structure that does not change its shape or intensity, although the input power is increased, as expected for dissipative solitons. The striations observed in the experimental pictures were found to be the effect of sample defects inside the waveguide. The sample facets were checked for defects by imaging after cleaving, and only perfectly cleaved samples have been used. It was

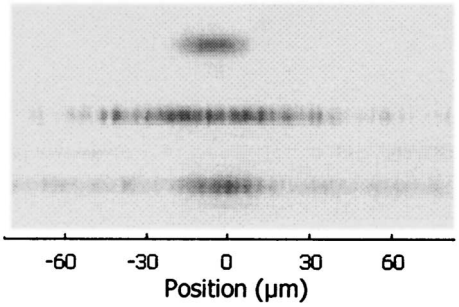

FIG. 2. (Top) Input beam profile at $\lambda = 965$ nm, Gaussian fitted FWHM = 16.5 μm. (Middle) Diffracted beam (62.5 μm FWHM) at the output facet. (Bottom) Output beam profile at $\lambda = 950$ nm, and 4A current injection.

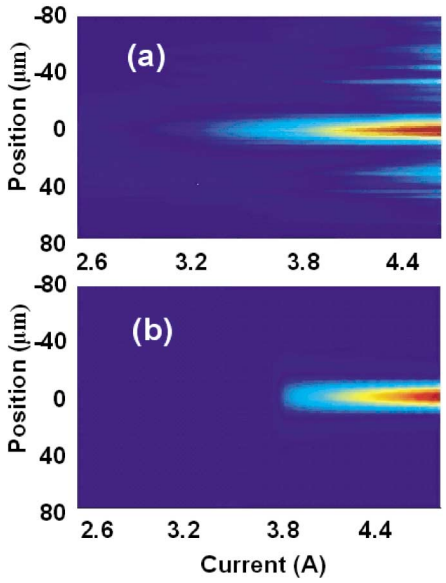

FIG. 3 (color online). (a) Images from output facet when the measured input at the focus of the microscope objective is 160 mW and 16.5 mm FWHM. Note that losses due to Fresnel reflection and mismatch between the Gaussian input beam and the waveguide mode reduce the power coupled into the waveguide. (b) Numerical simulation of the output profile with a 55 mW, 17.5 mm FWHM Gaussian assumed just inside the input facet of the waveguide.

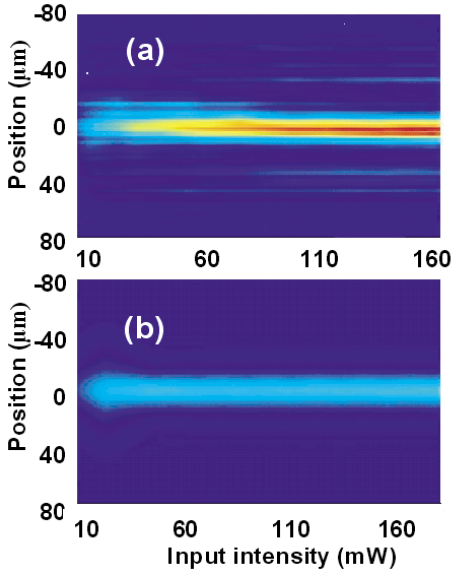

FIG. 4 (color online). (a) Images from the output facet with 4*A* pumping. (b) Numerical simulation of solitons at 4*A* pumping when the input intensity at the front facet is increased (50% coupling is assumed).

found that the stripe locations on the output image move with the sample when the sample is shifted perpendicular to the laser's propagation axis. Therefore they are a consequence of localized intrinsic defects in the waveguide. Numerical simulations with FDBPM in Fig. 4(b) show that once the intensity exceeds the subcritical branch value for a given pumping current, the soliton does not change its intensity or width as observed in the experiment.

We have also analyzed the change in output beam waist by increasing the input beam waist from 7 μm FWHM to 60 μm FWHM (Fig. 5). For an input beam waist smaller than 13 μm, the beam diffracts very fast, and numerical simulations show that it gets totally absorbed if the propagation continues after 1 cm device length. From 15 to 35 μm input FWHM, a stable localized soliton without a significant change in the output beam waist is formed. Larger input beam waist coupling does not give any soliton for a 1 cm device length, since the diffraction length at these beam waists is greater than 1 cm. However, numerical simulations suggest that for longer propagation distances, formation of multisolitonic structures is possible.

We investigated six different devices from the same wafer. All of them gave essentially the same output images for similar conditions. Thus we believe these solitons are very robust since dissipative solitons are strong attractors in these systems [3].

In conclusion, we have observed for the first time stable spatial dissipative solitons in a semiconductor optical amplifier device. Numerical simulations fit very well with the experiment results. With input powers of about

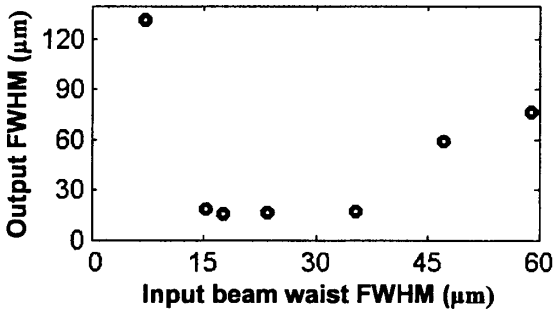

FIG. 5. Output beam waist versus the waist of a Gaussian input beam with 160 mW input power at front facet, and 4*A* current injection.

60 mW for excitation, these solitons are very exciting for potential soliton applications.

This research was supported by an ARO MURI titled "Solitonic Gateless Computing."

*Also with Fraunhofer Institut Jena, Winzerlaer Strasse 10, 07745 Jena, Germany.

[1] M. C. Cross and P. C. Hohenberg, Rev. Mod. Phys. **65**, 851 (1993).
[2] S. Trillo and W. Torruellas, *Spatial Solitons* (Springer, New York, 2001).
[3] N. N. Akhmediev and A. Ankiewicz, *Solitons: Nonlinear Pulses and Beams* (Chapman and Hall, London, 1997).
[4] IEEE J. Quantum Electron. **39** (2002); Feature section on spatial solitons (Issue 1) and cavity solitons (Issue 2).
[5] G. I. Stegeman and M. Segev, Science **286**, 1518 (1999).
[6] S. Barland *et al.*, Nature (London) **419**, 699 (2002).
[7] V. B. Taranenko, I. Ganne, R. Kuszelewicz, and C. O. Weiss, Phys. Rev. A **61**, 063818 (2000).
[8] D. Mehuys, R. J. Lang, M. Mittelstein, J. Salzaman, and A. Yariv, IEEE J. Quantum Electron. **23**, 1909 (1987).
[9] A. H. Paxton and G. C. Dente, J. Appl. Phys. **70**, 2921 (1991).
[10] L. Goldberg, M. R. Surette, and D. Mehuys, Appl. Phys. Lett. **62**, 2304 (1993).
[11] G. Khitrova *et al.*, Phys. Rev. Lett. **70**, 920 (1993).
[12] E. A. Ultanir, D. Michaelis, F. Lederer, and G. I. Stegeman, Opt. Lett. **28**, 251 (2003).
[13] S. Fauve and O. Thual, Phys. Rev. Lett. **64**, 282 (1990).
[14] S. Longhi and A. Geraci, Appl. Phys. Lett. **67**, 3062 (1995).
[15] S. V. Federov, A. G. Vladimirov, G. V. Khodova, and N. N. Rosanov, Phys. Rev. E **61**, 5814 (2000).
[16] G. P. Agrawal, J. Appl. Phys. **56**, 3100 (1984).
[17] S. Kristjansson, N. Eriksson, P. Modh, and A. Larsson, IEEE J. Quantum Electron. **37**, 1441 (2001).
[18] D. J. Bossert and D. Gallant, IEEE Photonics Technol. Lett. **8**, 322 (1996).
[19] K. Okamoto, *Fundamentals of Optical Waveguides* (Academic Press, San Diego, 2000).